

**Correlation of Electron Tunneling and Plasmon Propagation in a Luttinger Liquid**

Sihan Zhao,<sup>1,†</sup> Sheng Wang,<sup>1,2,†</sup> Fanqi Wu,<sup>3</sup> Wu Shi,<sup>1,2</sup> Iqbal Bakti Utama,<sup>1,2,4</sup> Tairu Lyu,<sup>1</sup> Lili Jiang,<sup>1</sup>  
 Yudan Su,<sup>5</sup> Siqi Wang,<sup>6</sup> Kenji Watanabe,<sup>7</sup> Takashi Taniguchi,<sup>7</sup> Alex Zettl,<sup>1,2,8</sup>  
 Xiang Zhang,<sup>2,6,9</sup> Chongwu Zhou,<sup>3,10,\*</sup> and Feng Wang<sup>1,2,8,\*</sup>

<sup>1</sup>*Department of Physics, University of California at Berkeley, Berkeley, California 94720, USA*

<sup>2</sup>*Materials Science Division, Lawrence Berkeley National Laboratory, Berkeley, California 94720, USA*

<sup>3</sup>*Department of Chemical Engineering and Materials Science, University of Southern California, Los Angeles, California 90089, USA*

<sup>4</sup>*Department of Materials Science and Engineering, University of California at Berkeley, Berkeley, California 94720, USA*

<sup>5</sup>*Department of Physics, State Key Laboratory of Surface Physics and Key Laboratory of Micro- and Nano-Photonic Structure (MOE), Fudan University, Shanghai 200433, China*

<sup>6</sup>*NSF Nanoscale Science and Engineering Center (NSEC), University of California at Berkeley, Berkeley, California 94720, USA*

<sup>7</sup>*National Institute for Materials Science, 1-1 Namiki, Tsukuba 305-0044, Japan*

<sup>8</sup>*Kavli Energy NanoSciences Institute at the University of California, Berkeley and Lawrence Berkeley National Laboratory, Berkeley, California 94720, USA*

<sup>9</sup>*Department of Physics, King Abdulaziz University, Jeddah 21589, Saudi Arabia*

<sup>10</sup>*Department of Electrical Engineering, University of Southern California, Los Angeles, California 90089, USA*



(Received 1 March 2018; published 27 July 2018)

Quantum-confined electrons in one dimension behave as a Luttinger liquid. However, unambiguous demonstration of Luttinger liquid phenomena in single-walled carbon nanotubes (SWNTs) has been challenging. Here we investigate well-defined SWNT cross junctions with a point contact between two Luttinger liquids and combine electrical transport and optical nanoscopy measurements to correlate completely different physical properties (i.e., the electron tunneling and the plasmon propagation) in the same Luttinger liquid system. The suppressed electron tunneling at SWNT junctions exhibits a power-law scaling, which yields a Luttinger liquid interaction parameter that agrees quantitatively with that independently determined from the plasmon velocity based on the near-field optical nanoscopy.

DOI: 10.1103/PhysRevLett.121.047702

A most fascinating phenomenon in one dimension (1D) is the Luttinger liquid physics, which establishes a new paradigm of a strongly correlated electron system distinctly different from a Fermi liquid. A Luttinger liquid represents the strongly coupled many-fermion system that is exactly solvable, and it exhibits many unusual physical properties: the Luttinger liquid is characterized by a power-law decay of the correlation functions and by spin-charge separation, where the spin and charge degrees of freedom propagate with different velocities [1–4]. Both the power indexes of the correlation function and the velocity ratio between charge and spin modes are uniquely defined by a single Luttinger liquid interaction parameter (hereafter Luttinger parameter)  $g$ . There has been tremendous and still ongoing efforts to probe the unusual Luttinger liquid physics in the past two decades [5–14]. However, there are often ambiguities in the interpretation because the unknown Luttinger parameter is often simply used as a fitting parameter [5–7,10,15]. An ultimate parameter-free test of the Luttinger liquid theory is highly desirable. This can be achieved by correlating completely different physical properties in the Luttinger liquid, because they are determined by the same Luttinger parameter  $g$ .

Single-walled carbon nanotubes (SWNTs), with diameters around 1 nm and lengths of microns to millimeters, provide ideal experimental realizations of the Luttinger liquid [5–7,15–18]. Previously, Luttinger liquid behavior in SWNTs has been mostly studied through electrical tunneling measurements in nanotubes and their ropes [5,7], which shows power-law-like tunneling probability. However, that interpretation is plagued by the unknown structure of the SWNT-metal contact tunnel junction and the unknown Luttinger parameter of nanotube ropes. Two crossed metallic SWNTs provide an attractive realization of the Luttinger liquid tunnel junction [19]. However, a previous study of crossed nanotubes with unknown physical properties reported a  $g$  value ( $g \sim 0.16$ ) much smaller than the theoretical prediction [16,17,20]. Here we investigate SWNT cross junctions with high quality that are directly grown on hexagonal boron nitride ( $h$ -BN) flakes. Using the recently developed near-field optical nanoscopy technique [21–25], we directly image the Luttinger liquid plasmons of the nanotubes on  $h$ -BN. This plasmon oscillation provides unambiguous identification of individual metallic SWNTs and directly yields an experimental determination of the Luttinger parameter  $g$  of the SWNT. We further carry out

low-temperature electrical transport measurements of the metallic SWNT cross junctions characterized by the near-field optical nanoscopy. We observe a constant power-law scaling in the electron tunneling current as a function of both electrical bias and temperature. The electrical tunneling between the two SWNTs has a gate-independent power index that corresponds to an average  $g$  value of  $\sim 0.30$ . It agrees quantitatively with the  $g$  values of the two constituent individual metallic SWNTs, which are independently determined from the plasmon velocity based on near-field optical nanoscopy. In contrast, isolated metallic SWNTs with metal contacts also exhibit apparent power-law scaling behavior, but the power index varies between different SWNTs and often yields a Luttinger parameter different from that determined through optical nanoscopy. It highlights the importance of combined electrical and optical study of well-defined tunneling junctions to quantitatively probe the Luttinger liquid phenomena.

High quality SWNT samples were directly grown on  $h$ -BN flakes exfoliated on  $\text{SiO}_2/\text{Si}$  substrate by a chemical vapor deposition method [26]. Plasmons in individual SWNTs were probed using infrared near-field optical nanoscopy with infrared light at  $\lambda_0 = 10.6 \mu\text{m}$  focusing on the apex of a metallic atomic force microscopy (AFM) tip. SWNT cross junction devices were fabricated using standard  $e$ -beam lithography with Pd/Au metal contacts (see device in the Supplemental Material, Sec. 1 [27]).

Figure 1 shows a representative SWNT cross junction sample on  $h$ -BN scanned by AFM. The cross junction comprises two individual SWNTs with a point contact. These types of cross junctions are formed on  $h$ -BN during the growth and can be occasionally found by the AFM scanning.

We observe well-defined Luttinger liquid plasmon oscillations with a high quality factor in individual metallic SWNTs on  $h$ -BN by using the near-field optical nanoscopy as shown in Fig. 2(a). Oscillation peaks in Fig. 2(a) correspond to the constructive interference between the excited plasmons under the tip and the reflected plasmon waves by the tube end. Therefore, the plasmon wavelength  $\lambda_p$  is simply two times the oscillation period of the near-field

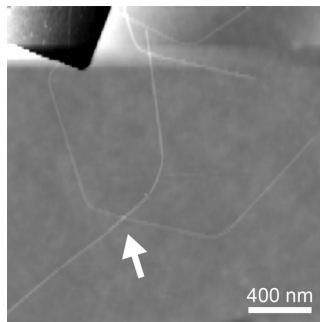


FIG. 1. AFM topography image of a representative SWNT cross junction sample (indicated by the arrow) on  $h$ -BN.

signal. We determine  $\lambda_p$  and quality factor  $Q$  by fitting the experimental plasmon oscillation profile in Fig. 2(a) (between two white bars) with the damped oscillator form  $e^{-2\pi x/(Q\lambda_p)} \sin[(4\pi x)/\lambda_p]$ . The results are presented in Fig. 2(b). The fitting can reproduce the experimental data very well, which yields  $\lambda_p = 90 \text{ nm}$  and  $Q = 25$ . Very importantly, the Luttinger parameter  $g$  can be directly obtained without relying on other parameters to be  $g \sim 0.31$  for this metallic SWNT by using  $1/g = v_p/v_F$ , where  $v_F \sim 8 \times 10^5 \text{ m/s}$  is the Fermi velocity of metallic SWNTs and  $v_p = c \times \lambda_p/\lambda_0 \sim 2.6 \times 10^6 \text{ m/s}$  is the plasmon velocity [24]. Note that we observe consistent Luttinger liquid plasmon oscillations and Luttinger parameters in all of our investigated individual metallic SWNT samples on  $h$ -BN.

We employ near-field optical nanoscopy to identify metallic SWNTs from semiconducting species in order to find SWNT cross junctions composed of two metallic

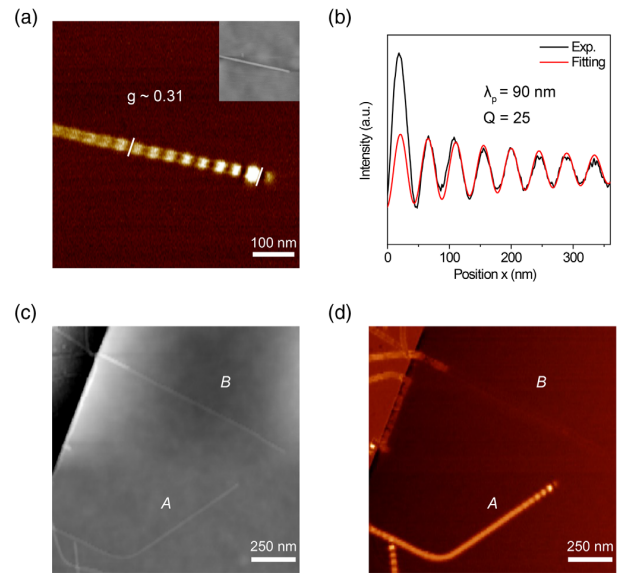


FIG. 2. Near-field optical nanoscopy characterizations on SWNTs on  $h$ -BN. (a) Near-field optical nanoscopy image of an individual metallic SWNT with a diameter of  $\sim 1 \text{ nm}$ . (Inset) Corresponding topography image that is simultaneously recorded. (b) Experimental intensity profile (in black) of Luttinger liquid plasmon oscillations and the corresponding theoretical fitting (in red) with the damped oscillator form  $e^{-2\pi x/(Q\lambda_p)} \sin[(4\pi x)/\lambda_p]$  along the tube axis between two bars in (a), where  $\lambda_p$  is the plasmon wavelength and  $Q$  is the quality factor. Luttinger parameter  $g \sim 0.31$  [shown in (a)] is directly obtained from the measured plasmon wavelength  $\lambda_p$ . (c) AFM topography image of an individual metallic SWNT (tube A) and an individual semiconducting SWNT (tube B) on  $h$ -BN with similar diameters  $\sim 0.8 \text{ nm}$ . (d) The corresponding near-field optical nanoscopy image of (c). The metallic SWNT (tube A) exhibits prominent Luttinger liquid plasmon oscillations, whereas the semiconducting SWNT (tube B) barely shows any near-field optical response owing to the finite band gap.

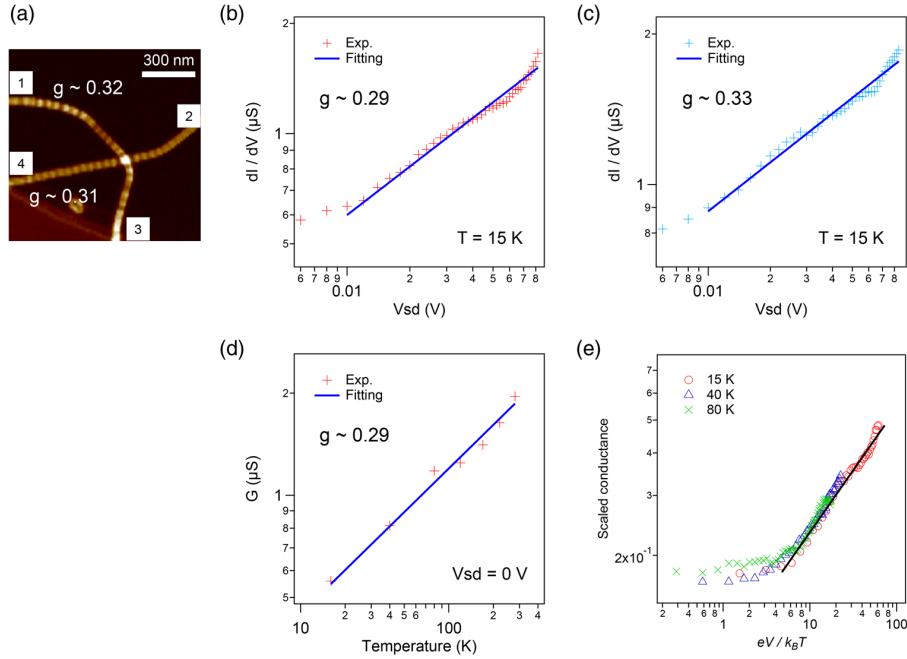


FIG. 3. Correlation of electron tunneling and plasmon propagation in a Luttinger liquid (device no. 1). (a) Near-field optical nanoscopy characterization on a metallic SWNT cross junction. Luttinger parameters are determined to be  $g \sim 0.32$  (tube 1-3) and  $g \sim 0.31$  (tube 2-4) for each of two nanotubes from the measured Luttinger liquid plasmons. Metal contacts are denoted by numbers. (b)  $dI/dV$  measurement of the electron tunneling probability across the Luttinger liquid junction as a function of electrical bias ( $Vsd$ ) at 15 K (through contacts 1 and 4). The SWNT junction dominates the total resistance and a two probe measurement is carried out. A power function fitting (blue line) yields the power index  $\alpha \sim 0.43$ , which corresponds to  $g \sim 0.29$  by using Eq. (1). (c) Power-law scaling behavior on electrical bias at 15 K at a different backgate voltage with respect to (b), which yields  $g \sim 0.33$ . (d) The corresponding temperature-dependent electron tunneling data (zero  $Vsd$ ) with the same backgate voltage as in (b), which yields  $g \sim 0.29$ . (e) Scaled conductance  $(dI/dV)/T^\alpha$  as a function of  $eV/k_B T$  at different temperatures, where  $\alpha$  is the power component with bias scaling at each temperature. All data collapse onto a single curve reasonably well, which provides an independent verification of Luttinger liquid behavior.

SWNTs because they exhibit very different Luttinger behaviors [28]. As an example, Figs. 2(c) and 2(d) present the topography image and the corresponding near-field optical nanoscopy image of two individual SWNTs with similar diameters  $\sim 0.8$  nm on  $h$ -BN, respectively. Nanotube *A* in Fig. 2(d) that exhibits Luttinger liquid plasmon oscillations corresponds to a metallic SWNT with zero band gap, whereas nanotube *B*, which is dark, is a semiconducting SWNT with a finite band gap. We further confirm this by complementary electrical transport measurements (see Supplemental Material, Sec. 2 [27]) [29]. We observe consistent results in all examined SWNT samples on  $h$ -BN.

Three metallic SWNT cross junctions characterized by near-field optical nanoscopy are shown in Fig. 3(a) (device no. 1), Supplemental Material, Sec. 5 (device no. 2), and Fig. 4(a) (device no. 3). A SWNT cross junction consisting of one metallic SWNT crossing another semiconducting SWNT is compared (see Supplemental Material, Sec. 3 [27]).

Our near-field optical nanoscopy characterization in Fig. 3(a) directly yields Luttinger parameters of the two

metallic tubes,  $g \sim 0.32$  (tube 1-3 between the electrical contacts 1 and 3) and  $g \sim 0.31$  (tube 2-4 between the electrical contacts 2 and 4), respectively, by the same analysis demonstrated in Fig. 2(b). We then independently obtain Luttinger parameter  $g$  on the same SWNT cross junction through measuring the electron tunneling probability across two Luttinger liquids by the electrical transport measurements. The results of device no. 1 are presented in Figs. 3(b)–3(e). The resistance of the two individual SWNT devices (1-3 and 2-4) both are  $\sim 50$  k $\Omega$  at room temperature, which is about 10 times smaller than that of the junction (e.g., 1-4). Since the junction dominates the total resistance (see Supplemental Material, Sec. 4), we measure the electron tunneling process across the junction in a two probe configuration between contacts 1 and 4 with contacts 2 and 3 floating. Figure 3(b) shows the measured  $dI/dV$  as a function of electrical bias  $Vsd$  in a double-logarithmic scale across the Luttinger tunneling junction (through contacts 1 and 4) at 15 K. The electron tunneling density of states in a Luttinger liquid is characterized by a power-law decay of correlation functions with the decrease of excitation energy (this case is the applied bias) in which the

measured  $dI/dV$  should scale with  $dI/dV \propto V^\alpha$ , where  $\alpha$  is an interaction- $(g)$ -dependent parameter to be determined. For electron tunneling from one Luttinger liquid to another, theory predicts that the power component  $\alpha$  is related to  $g$  as

$$\alpha = (g + 1/g - 2)/4. \quad (1)$$

Indeed, the experimentally observed  $dI/dV$  across the Luttinger liquid junction [red crosses in Fig. 3(b)] exhibits a well-defined power-law scaling [experimental fitting by blue line in Fig. 3(b)], which yields  $\alpha \sim 0.43$  and the corresponding  $g \sim 0.29$  by using Eq. (1). The power-law index shows a universal behavior, which remains a constant (within the experimental uncertainty) for electrical bias dependence at different backgate voltages and for temperature dependence. Figure 3(c) shows the electrical bias scaling behavior (through contacts 1 and 4) at a different backgate voltage at 15 K; experimental fitting by a power function (blue line) yields  $g \sim 0.33$ . The same power-law scaling behavior as in Fig. 3(b) (with the same backgate voltage) is observed in its corresponding temperature-dependent tunneling data, as presented in Fig. 3(d) ( $G \propto T^\alpha$  with zero  $V_{sd}$ ), which yields  $g \sim 0.29$ . This is consistent with Luttinger liquid prediction for metallic SWNTs with linear band dispersion with a constant tunneling barrier. We also directly measure the  $dI/dV$  at different temperatures, which provides an additional verification of Luttinger liquid behavior for electron tunneling across the SWNT junction. To see this, by following previous reports [5,7], we present our  $dI/dV$  results at different temperatures (15, 40, and 80 K) in Fig. 3(e), where the measured  $dI/dV$  is scaled by  $T^\alpha$  and the bias voltage is scaled by the thermal energy  $k_B T$ . If the experimental results agree with Luttinger liquid theory, all data at different temperatures should be able to collapse onto a single universal curve. As can be seen (eye guided by solid line) in Fig. 3(e), our data at different temperatures indeed collapse onto a single curve reasonably well. The quantitative agreement of Luttinger parameters, that is,  $g$  close to  $\sim 0.30$ , independently measured from electron tunneling density of states and plasmon propagation velocity in the same well-defined Luttinger liquid system, provides an unambiguous demonstration of Luttinger liquid behaviors in SWNTs. This is the first experimental correlation of different interaction-determined Luttinger liquid physical properties in the same carbon nanotube.

Correlation of electron tunneling and plasmon propagation were also carried out in two other SWNT cross junctions. The results of the second device (device no. 2) are shown in Supplemental Material, Sec. 5. The values of  $g$  obtained from the electrical tunneling and the plasmon oscillation agree nicely with each other, similar to that observed in device no. 1.

Experimental data of the third device (device no. 3) are displayed in Fig. 4. The Luttinger parameters for the two

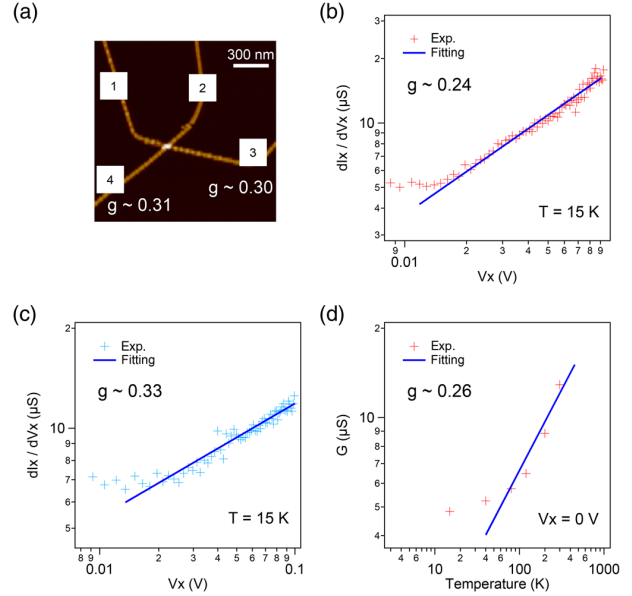


FIG. 4. Correlation of electron tunneling and plasmon propagation in a Luttinger liquid (device no. 3). (a) Near-field optical nanoscopy characterization on a metallic SWNT cross junction. Luttinger parameters are determined to be  $g \sim 0.30$  (tube 1-3) and  $g \sim 0.31$  (tube 2-4), respectively. Metal contacts are denoted by numbers. (b) Differential conductance ( $dI_x/dV_x$ ) measurement of the electron tunneling probability across the Luttinger liquid junction as a function of voltage drop across the junction ( $V_x$ ) at 15 K. Measurements are carried out in a four probe configuration where the electric current is forced to flow through contacts 1 and 2 and voltage drop is measured through contacts 3 and 4. A power function fitting (blue line) yields  $g \sim 0.24$  by using Eq. (1). (c)  $dI_x/dV_x$  at 15 K at a different backgate voltage with respect to (b), which yields  $g \sim 0.33$ . (d) The corresponding temperature-dependent electron tunneling data (zero  $V_x$ ) with the same backgate voltage as in (b), which yields a best fit of  $g \sim 0.26$ .

constituent metallic SWNTs are determined to be  $g \sim 0.30$  (tube 1-3) and  $g \sim 0.31$  (tube 2-4) as presented in Fig. 4(a) based on the near-field optical nanoscopy characterizations. The resistance for tube 1-3 and tube 2-4 is  $\sim 50$  and  $\sim 60$  k $\Omega$  at room temperature, and the resistance for the SWNT junction is  $\sim 80$  k $\Omega$  by a four probe measurement. The four probe tunneling measurement is achieved by forcing current to flow through contacts 1 and 2 and using contacts 3 and 4 as voltage probes. We first measure the electron tunneling density of states  $dI_x/dV_x$  as a function of voltage drop  $V_x$  across the junction at 15 K. The data are plotted in Fig. 4(b) with a double-logarithmic scale. An apparent power-law scaling of tunneling conductance  $dI_x/dV_x \propto (V_x)^\alpha$  across the Luttinger liquid tunneling junction is observed. Experimental fitting by a power function (blue line) yields an effective  $g$  value of  $\sim 0.24$ . The corresponding temperature-dependent data exhibits a  $g$  value close to

$\sim 0.26$  [Fig. 4(d)], while the electrical bias scaling behavior at a different backgate voltage yields a best fit value of  $g \sim 0.33$  [Fig. 4(c)]. In this device, the  $g$  values are close to the Luttinger parameters ( $g$  close to  $\sim 0.30$ ) obtained from the plasmon velocity measurements on the same Luttinger liquid [Fig. 4(a)], but they show a finite variation in different measurements. Presumably, this apparent  $g$  value variation from 0.24 to 0.33 is due to a small change of the tunneling coefficient as a function of the electrical bias and/or temperature that is caused by nanotube deformations under bias conditions. At present, we do not understand the microscopic origin of the small  $g$  variation observed from electrical tunneling in device no. 3. It highlights the importance of combined electrical and optical characterizations in order to obtain quantitative determination of the Luttinger parameter  $g$ .

Interestingly, the  $dI/dV$  measurement on the constituent individual metallic SWNT (e.g., tube 1-3 in Fig. 3) also exhibits an apparent power-law scaling of tunneling density of states (see Supplemental Material, Sec. 4), which is similar to that reported in previous studies [5,7]. The power index  $\alpha$  is related to  $g$  as

$$\alpha = (1/g - 1)/4 \quad (2)$$

for electron tunneling between metal contacts and SWNTs underneath them [5,16,17]. Fitting the experimental data by a power function yields  $\alpha \sim 0.11$  and  $g \sim 0.70$ , which deviates significantly from the measured  $g \sim 0.32$  by the near-field optical nanoscopy [Fig. 3(a)]. Measurements on other isolated individual metallic SWNTs show that the power scaling index varies in different SWNTs significantly (see Supplemental Material, Sec. 4 [27]), although the optically determined Luttinger parameter remains the same. We attribute this variation to the complicated and unknown nature of SWNT-metal contacts, which can modify the electron tunneling process in an uncontrolled fashion and mask the underlying Luttinger liquid behavior.

In summary, we directly correlate two completely distinct physical properties, i.e., the electron tunneling density of states and the plasmon propagation velocity in the same SWNT cross junctions, to obtain the first definitive parameter-free test of the Luttinger liquid phenomena in carbon nanotubes. Our combined electrical and optical studies can open up new opportunities for quantitative understanding of Luttinger liquid physics in SWNTs and other 1D systems.

This work was mainly supported by the Director, Office of Science, Office of Basic Energy Sciences, Materials Sciences and Engineering Division of the U.S. Department of Energy under Award No. DE-AC02-05-CH11231 (Subwavelength Metamaterial Program). Electrical transport measurements were supported by the Office of Naval

Research (MURI Grant No. N00014-16-1-2921). F. Wu and C. Z. acknowledge King Abdulaziz City for Science and Technology (KACST) for financial support. K. W. and T. T. acknowledge support from the Elemental Strategy Initiative conducted by the MEXT, Japan and JSPS KAKENHI Grant No. JP15K21722.

\*To whom correspondence should be addressed.  
fengwang76@berkeley.edu; chongwuz@usc.edu

†These authors contributed equally to this work.

- [1] J. M. Luttinger, *J. Math. Phys. (N.Y.)* **4**, 1154 (1963).
- [2] S.-i. Tomonaga, *Prog. Theor. Phys.* **5**, 544 (1950).
- [3] F. D. M. Haldane, *J. Phys. C* **14**, 2585 (1981).
- [4] T. Giamarchi, *Quantum Physics in One Dimension* (Oxford University Press, New York, 2004), Vol. 121.
- [5] M. Bockrath, D. H. Cobden, J. Lu, A. G. Rinzler, R. E. Smalley, L. Balents, and P. L. McEuen, *Nature (London)* **397**, 598 (1999).
- [6] H. Ishii *et al.*, *Nature (London)* **426**, 540 (2003).
- [7] Z. Yao, H. W. C. Postma, L. Balents, and C. Dekker, *Nature (London)* **402**, 273 (1999).
- [8] S. Tarucha, T. Honda, and T. Saku, *Solid State Commun.* **94**, 413 (1995).
- [9] A. Yacoby, H. L. Stormer, N. S. Wingreen, L. N. Pfeiffer, K. W. Baldwin, and K. W. West, *Phys. Rev. Lett.* **77**, 4612 (1996).
- [10] D. Laroche, G. Gervais, M. P. Lilly, and J. L. Reno, *Science* **343**, 631 (2014).
- [11] F. P. Milliken, C. P. Umbach, and R. A. Webb, *Solid State Commun.* **97**, 309 (1996).
- [12] A. M. Chang, L. N. Pfeiffer, and K. W. West, *Phys. Rev. Lett.* **77**, 2538 (1996).
- [13] M. Hashisaka, N. Hiyama, T. Akiho, K. Muraki, and T. Fujisawa, *Nat. Phys.* **13**, 559 (2017).
- [14] Y. Jompol, C. J. B. Ford, J. P. Griffiths, I. Farrer, G. A. C. Jones, D. Anderson, D. A. Ritchie, T. W. Silk, and A. J. Schofield, *Science* **325**, 597 (2009).
- [15] N. Y. Kim, P. Recher, W. D. Oliver, Y. Yamamoto, J. Kong, and H. Dai, *Phys. Rev. Lett.* **99**, 036802 (2007).
- [16] C. Kane, L. Balents, and M. P. A. Fisher, *Phys. Rev. Lett.* **79**, 5086 (1997).
- [17] R. Egger and A. O. Gogolin, *Phys. Rev. Lett.* **79**, 5082 (1997).
- [18] R. Saito, G. Dresselhaus, and M. S. Dresselhaus, *Physical Properties of Carbon Nanotube* (Imperial College Press, London, 1998).
- [19] A. Komnik and R. Egger, *Phys. Rev. Lett.* **80**, 2881 (1998).
- [20] B. Gao, A. Komnik, R. Egger, D. C. Glattli, and A. Bachtold, *Phys. Rev. Lett.* **92**, 216804 (2004).
- [21] Z. Fei *et al.*, *Nature (London)* **487**, 82 (2012).
- [22] J. Chen *et al.*, *Nature (London)* **487**, 77 (2012).
- [23] J.-H. Kang, S. Wang, Z. Shi, W. Zhao, E. Yablonovitch, and F. Wang, *Nano Lett.* **17**, 1768 (2017).
- [24] Z. Shi, X. Hong, H. A. Bechtel, B. Zeng, M. C. Martin, K. Watanabe, T. Taniguchi, Y.-R. Shen, and F. Wang, *Nat. Photonics* **9**, 515 (2015).
- [25] L. Jiang *et al.*, *Nat. Mater.* **15**, 840 (2016).

- [26] B. Liu, F. Wu, H. Gui, M. Zheng, and C. Zhou, *ACS Nano* **11**, 31 (2017).
- [27] See Supplemental Material at <http://link.aps.org/supplemental/10.1103/PhysRevLett.121.047702> for more data on sample characterizations and measurements.
- [28] A. Imambekov, T. L. Schmidt, and L. I. Glazman, *Rev. Mod. Phys.* **84**, 1253 (2012).
- [29] M. S. Purewal, B. H. Hong, A. Ravi, B. Chandra, J. Hone, and P. Kim, *Phys. Rev. Lett.* **98**, 186808 (2007).